ISSN: 0067-2904

The Dissipation of the Kinetic Energy for 2D Bounded Flow by Using Moment-Based Boundary Conditions with Burnett Order Stress for LBM

Seemaa A. Mohammed
Department of mathematics, University of Baghdad, Baghdad, Iraq

Received: 21/6/2023 Accepted: 19/9/2023 Published: 30/8/2024

Abstract

In this article, the lattice Boltzmann method with two relaxation time (TRT) for the D2Q9 model is used to investigate numerical results for 2D flow. The problem is performed to show the dissipation of the kinetic energy rate and its relationship with the enstrophy growth for 2D dipole wall collision. The investigation is carried out for normal collision and oblique incidents at an angle of 30°. We prove the accuracy of moment -based boundary conditions with slip and Navier-Maxwell slip conditions to simulate this flow. These conditions are under the effect of Burnett-order stress conditions that are consistent with the discrete Boltzmann equation. Stable results are found by using this kind of boundary condition where dissipation of the kinetic energy is found to be proportional to Re^{-1} in the first regime and it is $\propto Re^{-0.5}$ in the second part of the regime as expected. An excellent agreement with the benchmark data is observed.

Keywords:. Lattice Boltzmann, moment-based boundary conditions, Two relaxation times , kinetic energy

تبديد الطاقة الحركية للتدفق ثنائي الابعاد باستخدام طريقة الزخم الحدودية تحت تاثير برنيت باستخدام طريقة بولتزمان الشعرية

سيماء عبد الستار محمد

قسم الرياضيات ,كليه العلوم, جامعة بغداد, بغداد, العراق

الخلاصة

في هذا البحث ، يتم استخدام طريقة بولتزمان الشعرية لنموذج **D2Q9** لاستقصاء النتائج العددية للتدفق ثنائي الأبعاد. يتم تنفيذ المشكلة لإظهار تبديد معدل الطاقة الحركية وعلاقته بنمو مجموع التدويرات لمائع من نوع خاص. يتم إجراء التحقيق لتصادم عادي وتصادم مائل بزاوية 30 درجة. أثبتنا دقة شروط الحدودية مع عدم وجود انزلاق ووجود انزلاق ماكسويل و لمحاكاة هذا التدفق. تخضع هذه الشروط لتأثير ظروف إجهاد بورنيت التي تتوافق مع معادلة بولتزمان المنفصلة. تم الحصول على نتائج مستقرة باستخدام هذا النوع من الشروط الحدودية حيث يوجد تبديد للطاقة الحركية متناسبًا بطرق عكسيه مع متغير ريمان في النصف الاول من المجال ومع معكوس الجذري لنفس المتغير كما هو متوقع. لوحظ وجود توافق ممتاز مع البيانات المعيارية

*Email: Seemaa.a@sc.uobaghdad.edu.iq

1. Introduction

In the limit when the viscosity tends to zero, the dissipation of kinetic energy has been proposed mainly by Frag *et al* [1] for no-slip and free-slip boundaries. This study is carried out from numerical simulation to two-dimensional (2D) fluid flow, namely a dipole wall collision. In this numerical study, the dipole collided with the wall normally. Noting, many papers have investigated the dipole wall collision numerically for normal and oblique incidents for slip and no slip boundaries, like in [2-6]. The interaction between the two monopoles and the wall accompanies the generation of additional vortices at the wall. The production of small-scale vortices at the boundary leads to the decay of the kinetic energy caused by increasing the enstrophy at the wall. The study of this phenomena has been experimented on by a lot of authors. Clercx and Heijst [7] investigated the scaling of energy rate and the raise of the maximum enstrophy and Palinstrophy $P(t)$ for no slip bounded and unbounded domain. They show that owing to the production of the additional vortices at the wall, the energy scales proportional to $Re^{-0.5}$. The Reynolds number Re is defined as $Re = UH/\nu$ where U is the characteristic velocity and H is the half-width of the domain. Their examination happens for normal and oblique wall collisions in a range of Reynolds numbers between 500 and 128000. Keetels *et al.* [8] used an oscillating plate as a boundary layer to study the scales of enstrophy growth and Palinstrophy for no slip boundaries. Their investigation states that the enstrophy $\propto Re^{0.75}$ and $P(t) \propto Re^{2.25}$ for $Re < 20000$. For $Re \geq 20000$ the growth of enstrophy $\propto Re^{0.5}$ and $P(t) \propto Re^{1.5}$. Following Frag *et al* [1] and . Clercx and Heijst [7], and Sutherland [9] employed slip and no slip boundary conditions to examine the energy dissipation structure. Frag *et al* and Sutherland showed that Prandtl's theory [10] was satisfied for slip and various slip-length wall collisions. They showed that the slope $\propto 0.43$ for slip equal to $4/Re$ and no slip walls. For boundary with slip length equal to 0.003, the slope is equal to -0.53$\pm$0.05 . Clercx and Heijst [11] gave a detailed study and review of many investigations that deal with dipole wall collision and the scale of the dissipation of energy.

The papers above used traditional computational fluid dynamics (CFD) methods to investigate the scale of energy dissipation, which discretizes the Navier-Stokes equations directly, like finite difference, finite volume, finite elements and spectral methods and others [12-14]. Mohammed [15] used a method that avoided the difficulties where CFD methods are faced and reached out to the same results as Frag *et al* and Sutherland. These difficulties are summarized by computational expenses or complicities by applying the boundary methods, especially with slip conditions. This method is called the Lattice Boltzmann method (LBM). The LBM is an alternative to the CFD methods. Thus, the LBM has been obtained from the velocity space and discretizing the Boltzmann equation (BE)[16][17]. The first model of this method is called the Bhanagar-Gross-Krook (BGK-LBM) collision operator [17][18]. Because of a shortcoming of the BGK operator in terms of higher Reynolds numbers, a generalization of this model is found by d'Humieres [19] namely, the multiple relaxation time (MRT- LBM) operator. This operator gave more stability and accuracy to the LBM. A special case of MRT is the two relation time model (TRT-LBM). The stability of this model is ruled by one parameter the so called "magic parameter" Λ. For D2Q9 LB model by setting $\Lambda = \frac{1}{4}$, one can reach the numerical stability of the LBM [20-22].

One of the most important distinguishing features of LBM is the ease of applying the boundary conditions for simple and complex boundaries. The simplest method is "bounce back" boundary conditions. In this method, the velocity particles hit the wall and reverse their way to the fluid bulk [23][24]. However, for the accuracy of this method, a numerical error appeared with a second-order error if the wall is located midway between grid points and

first-order accuracy elsewhere. Alternatively, other methods were proposed as a modification of the bounce back method that depends on lattice velocity distribution function, like [25-28]. On the other hand, another approach was proposed by Noble *et al.* [29] that depends on the hydrodynamic moments of the LBM. This method was modified by Bennett [30] for the D2Q9 model, the so-called "Moment-based " boundary conditions. This method simulated simple and complex flows with slip and no slip boundaries accurately, like in [3][31-34]. The moment method is also employed to consider conditions that are proportional to the deviatoric stress which is used to estimate the non Navier-Stokes behavior for slip and no slip boundaries [35][36]. In this article, it is shown that the LBM with a consistent moment method with an effect of Burnett contribution can precisely compute and capture a dissipation of the kinetic energy with an enstrophy growth rate for slip and no slip boundaries for 2D bounded flow.

This article is organaised as follows:

In Section 2, we introduce the discrete Boltzmann equation (DBE). In Section 3,4 we show the macroscopic moments of DBE, then we discuss the lattice Boltzmann algorithm. The TRT-LBM scheme is proposed in Section 5. In Section 6, we explain the moment-based boundary condition with the Burnett effect. Finally, in Section 7 numerical results are provided for the dissipation of the kinetic energy by using the boundary method from Section 6.

2. The discrete Boltzmann equation

In this section, the D2Q9 model will be presented for the discrete Boltzmann equation (DBE) as

$$\frac{df_j}{dt} + c_j \,.\nabla f_j = -\frac{1}{\tau}\left(f_j - f_j^0\right), \qquad \text{for } j = 0, \ldots, 8. \tag{1}$$

The advection part of the probability distribution function f_j is given in the left hand side of equation (1) with the discrete particle velocity $\boldsymbol{c}_j$. The D2Q9 model has 9 particle velocities c_j, as shown in Figure 1.

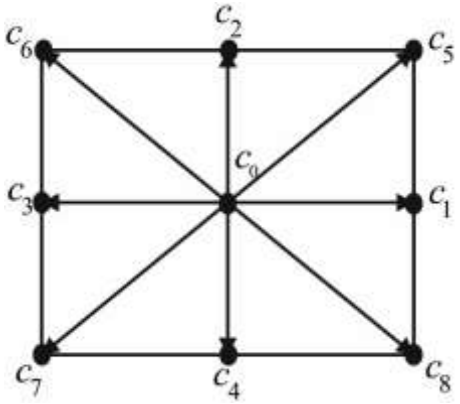

Figure 1: The D2Q9 lattice

The right hand side is the collision part that relaxes the distribution function into their local equilibrium f_j^0 with single relaxation time τ. The stipulated equilibria f_j^0can be defined from Maxwell Boltzmann equation as a function of fluid density ρ and macroscopic velocity $\boldsymbol{u}$ as [37],

$$f_j^0(\mathbf{x},t)=\omega_j\,\rho\left(1+\frac{c_j.\boldsymbol{u}}{c_s^2}+\frac{\left(c_j.\boldsymbol{u}\right)^2}{2c_s^4}-\frac{\boldsymbol{u}^2}{2c_s^2}\right), \tag{2}$$

where $c_s^2 = 1/3$ is the speed of sound for the D2Q9 LB model. The D2Q9 model weights is given by:

$$\omega_j = \begin{cases} \frac{4}{9}, & j = 0, \\ \frac{1}{9}, & j = 1, \dots, 4, \\ \frac{1}{36}, & j = 5, \dots, 8, \end{cases} \tag{3}$$

while the discrete lattice velocity are calculated from

$$\boldsymbol{c_j} = \begin{cases} (0,0), & j = 0, \\ \left(cos\frac{(j-1)\pi}{2}, sin\frac{(j-1)\pi}{2}\right), & j = 1,2,3,4, \\ \sqrt{2}\left(cos\frac{(2j-1)\pi}{4}, sin\frac{(2j-1)\pi}{4}\right), & j = 5,6,7,8. \end{cases} \tag{4}$$

The hydrodynamic variables which are, density(ρ), momentum ($\rho\boldsymbol{u}$) and momentum flux ($\boldsymbol{\Pi}$), are defined via a discrete moments of the distribution functions f_j

$$\rho = \sum_j f_j ; \qquad \rho\boldsymbol{u} = \sum_j f_j \, \boldsymbol{c}_j ; \qquad \boldsymbol{\Pi} = \sum_j f_j \, \boldsymbol{c}_j \boldsymbol{c}_j ; \tag{5}$$

The lasting three non-hydrodynamic moments (“ghost moments”) are presented by

$$Q_{xxy} = \sum_j f_j c_{jy} \, c_{jx}^2 , \qquad Q_{xyy} = \sum_j f_j c_{jx} \, c_{jy}^2 , \qquad S_{xxyy} = \sum_j f_j c_{jy}^2 \, c_{jy}^2 . \tag{6}$$

3. Macroscopic equations

The following evaluation equations are obtained by taking the zeroth, first and second order moment equations of the discrete Boltzmann equation (1), [24]

$$\frac{\partial \rho}{\partial t} + \nabla . \rho\boldsymbol{u} = 0, \tag{7}$$

$$\frac{\partial \rho\boldsymbol{u}}{\partial t} + \nabla . \boldsymbol{\Pi} = 0, \tag{8}$$

$$\frac{\partial \boldsymbol{\Pi}}{\partial t} + \nabla . \mathbf{Q} = -\frac{\mathbf{1}}{\tau}(\boldsymbol{\Pi} - \boldsymbol{\Pi^0}), \tag{9}$$

where $\mathbf{Q} = \sum_{\boldsymbol{j}} f_j \, \boldsymbol{c}_j \boldsymbol{c}_j \, \boldsymbol{c_j}$ and $\boldsymbol{\Pi^0}$=$\sum_{\boldsymbol{j}} f^0{}_j \, \boldsymbol{c}_j \boldsymbol{c}_j$ declares that the momentum flux relaxes into its equilibrium which is obtained from equation (2), such that

$$\boldsymbol{\Pi^0} = \frac{\rho}{\mathbf{3}}\boldsymbol{I} + \rho\boldsymbol{uu}. \tag{10}$$

The ideal equation of the state gives the pressure equation $P = \frac{\rho}{3}$.

By using the Chapman–Enskog expansion [38], the equations of motion can be obtained from the Boltzmann equation, which aims for solution for a long timescale, extremely longer than τ. In other way, the deviatoric stress $\boldsymbol{\Omega} = \boldsymbol{\Pi} - \boldsymbol{\Pi^0}$, which is the right hand side of equation (9), can be used by applying a methodology was proposed by Maxwell to get the Navier-Stokes equations [15]. To do this, one can take moments regarding a velocity which is defined as a difference between the fluid velocity and the particle velocity, such that $\boldsymbol{\xi} = \boldsymbol{c_j} - \boldsymbol{u}$ [39]. The deviatoric stress for D2Q9 according to Dellar [36] can be written for equation (9) as

$$\Omega_{\alpha\beta} + \tau\left(\partial_t \, \Omega_{\alpha\beta} + u_\gamma \, \partial_\gamma \, \Omega_{\alpha\beta} + \Omega_{\alpha\gamma} \, \partial_\gamma u_\beta + \Omega_{\beta\gamma} \, \partial_\gamma u_\alpha \right) = \mu(\partial_\beta u_\alpha + \partial_\alpha u_\alpha), \tag{11}$$

Where $\mu = \rho\tau/3$ is the dynamic viscosity and α, β and γ are the Cartesian components of the vectors and tensors. Noting, the third order moment is equal to zero.
Equation (11) gives three components of the stress which are

$$\Omega_{\mathrm{xx}} + 2\tau\, \Omega_{xy}\, \frac{\partial u_x}{\partial y} = 0, \tag{12}$$

$$\Omega_{yy} = 0, \tag{13}$$

$$\Omega_{\mathrm{xy}} - \mu\ \frac{\partial u_x}{\partial y} = 0. \tag{14}$$

The normal component and the shear stress are given in equations (13) and (14), respectively. These two stresses are the same as in Navier-Stokes equations. However, the tangential stress from equation (12) is not as in the Navier-Stokes equations which should be vanished. Instead, it is proportional to the square of the shear stress at $\mathrm{O}(\tau^2)$ which is identical to the stress of the Burnett equation. Owing to this fact, a special treatment of the tangential stress at the boundary is considered in the lattice Boltzmann simulations.

4. The BGK lattice Boltzmann equation

Equation (1) is integrated for both sides along characteristic for time,Δt, to get

$$f_j\big(\boldsymbol{x} + \boldsymbol{c}_j\Delta t, t + \Delta t\big) - f_j(\boldsymbol{x}, t) = -\frac{1}{\tau}\int_0^{\Delta t}\big(f_j - f_j^0\big)ds. \tag{15}$$

The left side is evaluated exactly. By using the trapezoidal rule, the right hand side is approximated to get a second order with implicit system of equations

$$f_j\big(\boldsymbol{x} + \boldsymbol{c}_j\Delta t, t + \Delta t\big) - f_j(\boldsymbol{x}, t) = -\frac{\Delta t}{2\tau}\Big(f_j\big(\boldsymbol{x} + \boldsymbol{c}_j\Delta t, t + \Delta t\big) - f_j^0(\boldsymbol{x}, t)\Big) - \frac{\Delta t}{2\tau}\Big(f_j(\boldsymbol{x}, t) - f_j^0(\boldsymbol{x}, t)\Big) + \mathrm{O}(\Delta t^3). \tag{16}$$

Transformed functions are proposed by He et al. [40], to convert the second order implicit system of equations (16) to explicit algorithm, thus

$$\bar{f}_{\,j} = f_j(\boldsymbol{x}, t) + \frac{\Delta t}{2\tau}\Big(f_j(\boldsymbol{x}, t) - f_j^0(\boldsymbol{x}, t)\Big). \tag{17}$$

Substitute equation (17) into equation (16), *the Lattice Boltzmann equation* is recovered in term of $\bar{f}_{\,j}$

$$\bar{f}_{\,j}\big(\boldsymbol{x} + \boldsymbol{c}_j\Delta t, t + \Delta t\big) - \bar{f}_{\,j}(\boldsymbol{x}, t) = -\frac{\Delta t}{\left(\tau + \frac{\Delta t}{2}\right)}\Big(\bar{f}_{\,j}(\boldsymbol{x}, t) - \bar{f}^{\,0}{}_{j}(\boldsymbol{x}, t)\Big) + \mathrm{O}(\Delta t^3). \tag{18}$$

Mention that the lattice speed connect the grid space and time step by $c = (\Delta x/\Delta t) \gg 1$
The zeroth moment of equation (17) gives the density ρ,

$$\rho = \textstyle\sum_j f_j = \sum_j \bar{f}_{\,j}\,; \tag{19}$$

The first moment of equation (17) yields the momentum equation of motion in terms of $\bar{f}_{\,j}$

$$\rho\boldsymbol{u} = \textstyle\sum_j f_j\, \boldsymbol{c}_j = \sum_j \bar{f}_{\,j}\, \boldsymbol{c}_j\,. \tag{20}$$

While the non-conserved momentum flux is given by

$$\bar{\boldsymbol{\Pi}} = \textstyle\sum_j \bar{f}_{\,j}\, \boldsymbol{c}_j\boldsymbol{c}_j = \left(1 + \frac{\Delta t}{2\tau}\right)\boldsymbol{\Pi} - \frac{\Delta t}{2\tau}\boldsymbol{\Pi}^{\boldsymbol{0}}. \tag{21}$$

Consequently, the deviatoric stress $\boldsymbol{\Omega} = \boldsymbol{\Pi} - \boldsymbol{\Pi}^{\boldsymbol{0}}$ is given in terms of barred distribution functions as

$$\boldsymbol{\Omega} = \boldsymbol{\Pi} - \boldsymbol{\Pi}^{\boldsymbol{0}} = \frac{2\tau(\boldsymbol{\Pi}^{\boldsymbol{0}} - \bar{\boldsymbol{\Pi}})}{(2\tau + \Delta t)}. \tag{22}$$

5. Two Relaxation time lattice Boltzmann equation

The BGK-LBE model is an accurate model to simulate different kinds of numerical simulations. However, sometimes this model experienced a lack of numerical stability,

particularly with a high Reynolds number; because of $\bar{f}_j$ over relax their equilibria [41]. To solve this problem, instead of using one rate of collision time τ, one can use two relaxation times. The two Relaxation time (TRT) is a special model of multiple relaxation time (MRT) [19][41-43] . In general, the discrete Boltzmann equation gives the two relaxation time equations as follows

$$\frac{df_j}{dt} + \boldsymbol{c}_j \cdot \nabla f_j = -\frac{1}{\tau^+}\left(\frac{1}{2}\left(f_j + f_{\bar{j}}\right) - f_j^{0+}\right) - \frac{1}{\tau^-}\left(\frac{1}{2}\left(f_j + f_{\bar{j}}\right) - f_j^{0-}\right). \quad (23)$$

Equation (23) relaxes the odd and even moments at various rates. The even relaxation time τ^+ relaxes the even moments to its equilibria and τ^- is the relaxation rate for the odd moments. Moreover, $\bar{j}$ is the opposite way to j where $\boldsymbol{c}_{\bar{j}} = -\boldsymbol{c}_j$. The equilibrium function is divided into odd and even components f_j^{0+} and f_j^{0-} [44]. The Reynolds number controls the even relaxation time while τ^- is calculated by using the "magic parameter" $\Lambda = \tau^+\tau^-$. For numerical stability we set $\Lambda = 1/4$ [22].

Similar to Section 4, one can discretise equation (23) to get *Two relaxation lattice Boltzmann equation (TRT-LBE)*

$$\bar{f}_j\left(\boldsymbol{x} + \boldsymbol{c}_j\Delta t, t + \Delta t\right) = \bar{f}_j(\boldsymbol{x}, t) - \frac{\Delta t}{(\tau^+ + \Delta t/2)}\left(\frac{1}{2}\left(\bar{f}_j(\boldsymbol{x}, t) + \bar{f}_{\bar{j}}(\boldsymbol{x}, t)\right) - f_j^{0+}(\boldsymbol{x}, t)\right) - \frac{\Delta t}{(\tau^- + \Delta t/2)}\left(\frac{1}{2}\left(\bar{f}_j(\boldsymbol{x}, t) + \bar{f}_{\bar{j}}(\boldsymbol{x}, t)\right) - f_j^{0-}(\boldsymbol{x}, t)\right). \quad (24)$$

Noting if $\tau^+ = \tau^-$ in equation (24), BGK-LBM will be obtained.

6. Slip and no slip moment based boundary conditions based on Burnett contribution

For straight and aligned boundaries with grid points, there are three unknown distribution functions (the dash red lines in Figure 2) after every streaming step needed to be found at each boundary for the D2Q9 model, see Figure 2.

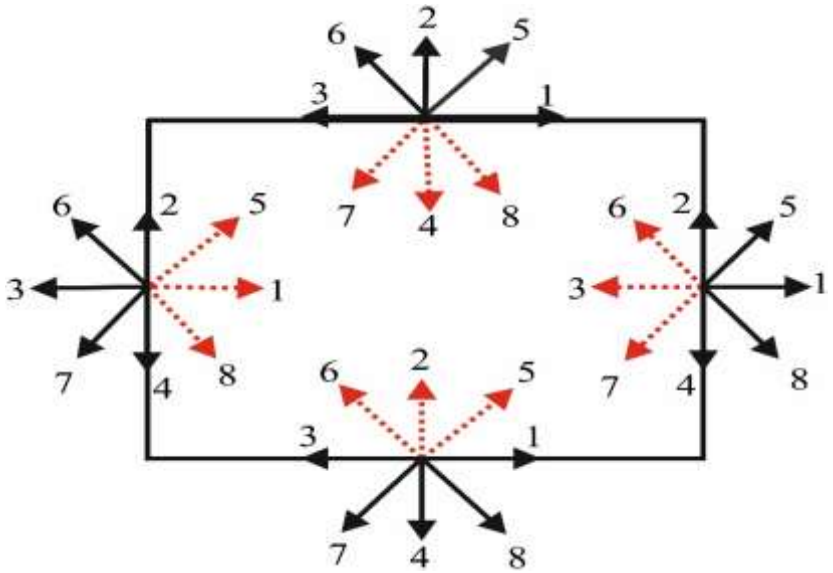

Figure 2: Distribution functions at the boundaries

To do this , Bennett [30] followed Noble et al.[29] by finding these unknown functions by imposing conditions on the three hydrodynamic moments at the boundary. This method is called " moment-based boundary condition" . Here we will explain this method for slip first then no slip conditions.

To understand the method let us investigate the tangential north wall. At the wall, the $x-$components of the velocity can be formulated with the Navier-Maxwell condition [45]. This condition illustrates that the tangential velocity is proportional to the shear stress at the planer wall, as

$$u_s = \varepsilon \frac{\partial u_x}{\partial y}\Big|_{wall}, \tag{25}$$

where ε indicates to slip length and y is the normal direction to the boundary.

Table 1: Combination of unknown at the north boundary

Moments	Combination of unknown at the north wall
$\bar{\rho}, \rho\bar{u}_y, \bar{\Pi}_{yy}$	$\bar{f}_4 + \bar{f}_7 + \bar{f}_8$
$\rho\bar{u}_x, \bar{\Pi}_{xy}, \bar{Q}_{xyy}$	$\bar{f}_7 - \bar{f}_8$
$\bar{\Pi}_{xx}, \bar{Q}_{xxy}, \bar{S}_{xxyy}$	$\bar{f}_7 + \bar{f}_8$

At the north wall, the three incoming functions that indicate into fluid domain $\bar{f}_4, \bar{f}_7$ and $\bar{f}_8$ need to be determined. In summary, since we have three unknown functions then three linearly independent moments should be used. It can be seen in Table-1, the unknown $\bar{f}_j$ appear in three linear combinations equations. In the moment method, one moment at each row will be picked and apply constraint on it, depending on the condition we use (slip, no slip, or free slip conditions). The moments will be appeared in terms of "barred" quantities. Since we simulate the Navier-Stokes equations, the rational choice is the hydrodynamic moments in lieu of higher-order moments. For slip walls, we will select from the first and second rows in the table ρu_y and ρu_x and apply conditions on them as

$$\rho u_y = 0,\ \rho u_x = \rho u_s\,, \tag{26}$$

while from the third row we will pick the tangential stress Π_{xx}.

To deal with the stresses we should mention that since this work includes TRT-LBE, the relaxation time depends on the even and odd rates, for more details see [35]. Applying equation (14) into equation (12) yields the tangential stress at the wall

$$\Omega_{xx} = -\frac{2\,\tau^-}{\mu}\ \Omega_{xy}^2, \tag{27}$$

where $\mu = \frac{\rho\tau^+}{3}$.

By the definition of equation (22), the tangential momentum flux can be defined as a relationship between the deviatoric stress and the tangential one as follows:

$$\bar{\Pi}_{xx} = \frac{\rho}{3} + \rho u_s^2 + \frac{2\tau^-}{\mu}\Omega_{xy}^2, \tag{28}$$

Using the transformation of $\bar{f}$ (17) gives the three converted hydrodynamic moments in equations as

$$\rho\bar{u}_y = 0,$$
$$\rho\bar{u}_s = \frac{3\lambda H}{\rho(2\,\tau^+ + 1)}\bar{\Pi}_{xy},$$
$$\bar{\Pi}_{xx} = \frac{\rho}{3} + \rho u_s^2 + \frac{6\tau^-}{\rho\left(\tau^+ + \frac{1}{2}\right)}\bar{\Pi}_{xy}^2, \tag{29}$$

where $\lambda = \varepsilon/H$ is the dimensionless slip length and the width of the domain is defined in terms of LB discretization as $H = H_n = (m_{lb} - 1)\Delta x$. It should be mentioned that the number of grid points is denoted by m_{lb} and the grid spacing is Δx.

By solving the above three equations, the three unknown functions $\bar{f}_4, \bar{f}_7, \bar{f}_8$ can be found in terms of known $\bar{f}_j$

$$\bar{f}_4 = \bar{f}_1 + \bar{f}_3 + \bar{f}_2 + 2(\bar{f}_5 + \bar{f}_6) - \frac{\rho}{3} - \rho u_s^2 - \frac{6\tau^-}{\rho\left(\tau^+ + \frac{1}{2}\right)}\bar{\Pi}_{xy}^2,$$

$$\bar{f}_7 = -\bar{f}_3 - \bar{f}_6 + \frac{\rho}{6} + \frac{1}{2}\rho u_s^2 - \frac{1}{2}\rho u_s + \frac{3\tau^-}{\rho\left(\tau^+ + \frac{1}{2}\right)}\bar{\Pi}_{xy}^2,$$

$$\bar{f}_8 = -\bar{f}_1 - \bar{f}_5 + \frac{\rho}{6} + \frac{1}{2}\rho u_s^2 + \frac{1}{2}\rho u_s + \frac{3\tau^-}{\rho\left(\tau^+ + \frac{1}{2}\right)}\bar{\Pi}_{xy}^2. \quad (30)$$

The moment density can be found by using the known $\bar{f}_j$ and the normal velocity $\rho\bar{u}_y$

$$\rho = \bar{f}_0 + \bar{f}_1 + \bar{f}_3 + 2(\bar{f}_2 + \bar{f}_5 + \bar{f}_6) - \rho\bar{u}_y, \quad (31)$$

where at the horizontal northern wall, $\rho\bar{u}_y = 0$.

The shear stress can be constructed at the boundary by applying the known $\bar{f}_j$ and the horizontal velocity $\rho\bar{u}_x$

$$\bar{\Pi}_{xy} = -\rho u_x + \bar{f}_1 - \bar{f}_3 + 2(\bar{f}_5 - \bar{f}_6). \quad (32)$$

Thus, together the shear stress of equation (32) and known distribution functions (31) can be used to find the tangential velocity at the wall

$$\bar{u}_s = \frac{6\lambda H\left(\bar{f}_1 - \bar{f}_3 + 2(\bar{f}_5 - \bar{f}_6)\right)}{\rho(2\tau^+ + 1 + 6\lambda H)}. \quad (33)$$

For no slip case, if we apply $u_x = 0$ at the wall, the no slip moment based boundary conditions with Burnett contribution will be found.

Finally for both cases, slip and no slip conditions, at the corners we need five constraints to find the unknown distribution functions. In our work, the no slip boundary conditions will be applied at the intersecting walls, For more details see [4] [33].

7. Numerical simulation of two-dimensional bounded flow

In this section, our aim is to show the scaling of the kinetic energy and the growth of the enstrophy for 2D flow using the boundary method that is presented in Section 6. To do this, firstly we will give a brief numerical study of dipole wall collision. This study is inserted to give an overview about the effect of the wall collision on the dissipation of the energy and its relationship with the increasing of the vortices production at the wall.

7.1 Initial setup and simulation parameters for 2D flow

The initial setup given here is similar to [2][3] as follows:

In a square box on a 2D domain with a size $[-1,1] \times [-1,1]$, the dipole wall collision has been studied by using TRT-LBE. This study is carried out with slip and no slip boundary conditions by using moment based with Burnett's contribution from section (6). Following [2], the initial characteristic velocities are defined by $U = \frac{1}{4}\iint |u|^2\, dx\, dy = 1$. The half width of the domain is considered to define the Reynolds number $Re = \frac{UH}{\nu}$. In the center of the cavity box, the initial two monopoles are located with the initial velocities

$$u_{x0} = -\frac{1}{2}|\omega_e|(y - y_1)\exp\left(-\left(\frac{r_1}{r_0}\right)^2\right) + \frac{1}{2}|\omega_e|(y - y_2)\exp\left(-\left(\frac{r_2}{r_0}\right)^2\right), \quad (34)$$

$$u_{y0} = \frac{1}{2}|\omega_e|(x - x_1)\exp\left(-\left(\frac{r_1}{r_0}\right)^2\right) - \frac{1}{2}|\omega_e|(x - x_2)\exp\left(-\left(\frac{r_2}{r_0}\right)^2\right), \quad (35)$$

where $r_1 = \sqrt{(x-x_1)^2+(y-y_1)^2}$, $r_2 = \sqrt{(x-x_2)^2+(y-y_2)^2}$, $r_0 = 0.1$. Also, $(x_1, y_1), (x_2, y_2)$ is the position of the vortex at the center of the domain, according to the angle of the incident while the strength of the vortices is set to be $|\omega_e| = 299.5$. Since our work shows the relationship between the kinetic energy and the total enstrophy by using the presented boundary method, then the following definitions are used

$$\textbf{Total kinetic energy: } E(t) = \frac{1}{2}\int_{-1}^{1}\int_{-1}^{1}|\boldsymbol{u}^2|(\boldsymbol{x},t)dx\,dy, \quad (36)$$

$$\textbf{Total enstrophy : : } \Omega(t) = \frac{1}{2}\int_{-1}^{1}\int_{-1}^{1}|\omega^2|(\boldsymbol{x},t)dx\,dy, \quad (37)$$

where the vorticity $\omega = \partial_x u_y - \partial_y u_x$. Noting, to normalise these to values, we set $E(0) = 2$ and $\Omega(0) = 800$. The convergent number of grid points m_{lb} is similar to the one in [3] . In [3][4] detailed explanations have been shown to the evaluation of two symmetric monopoles that collided with slip and no slip walls. These papers investigated the collision at normal and oblique incidents for different values of Reynolds numbers and boundary conditions. An evaluation of the flow is shown in Figure 3.

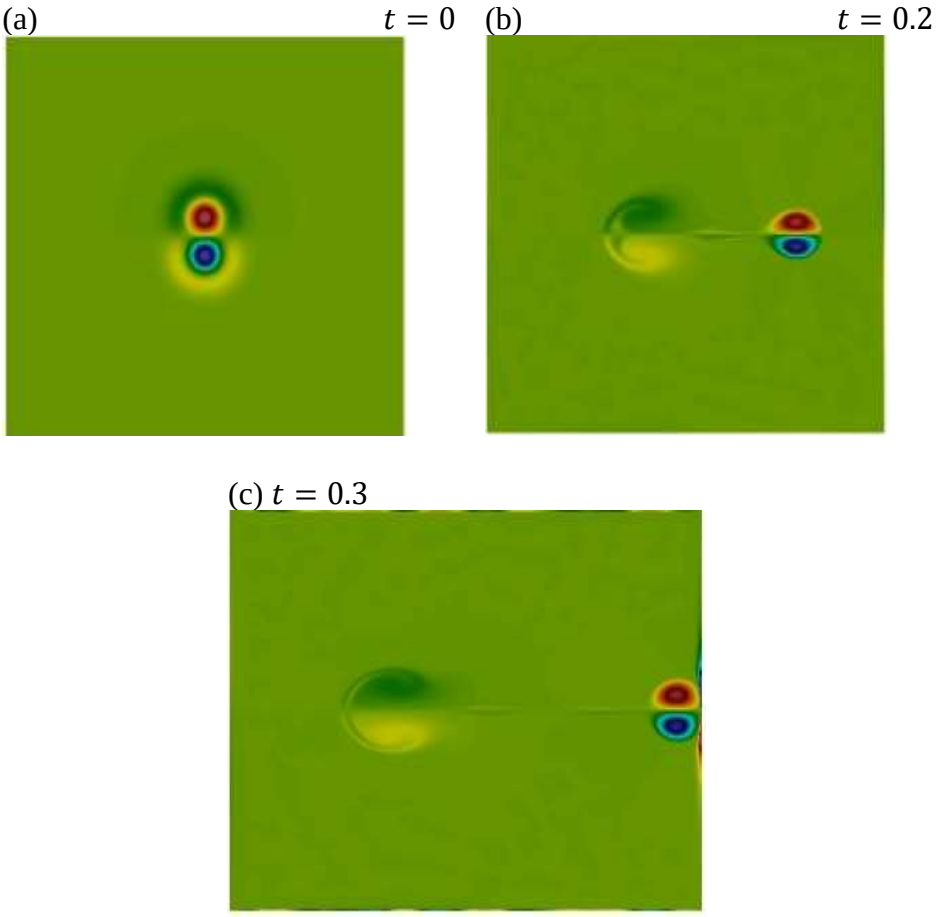

Figure 3: Vorticity contours of dipole wall collision at an angle of 0 for Re = 2500 .

This figure includes the initial stage at $t = 0$ until the first collision with no slip wall around $t = 0.3$ for $Re = 2500$ as an example. The two isolated monopoles are released from their shelf normally in the center of the domain at $t = 0$ towards $x = 1$. At the first wall collision, secondary dipoles are created at the same time the kinetic energy declines while the total enstrophy reaches its peak. In [4] we can notice that the total energy decreases by

increasing the slip length and the maximum enstrophy declines after the first wall collision with a higher slip length.
This leads to the following relationship for two-dimensional incompressible bounded flow. Within the slip wall, the relationship between the kinetic energy and the growth of the enstrophy is given by the following dimensionless equation [4]

$$\frac{dE}{dt} = -\frac{2}{Re}\Psi - \frac{1}{Re}\int_S (\omega \times \boldsymbol{u}).\boldsymbol{n}\ dS, \tag{38}$$

While for no slip walls, the above relationship will be reduced to not including the velocity part as

$$\frac{dE}{dt} = -\frac{2}{Re}\Psi \tag{39}$$

7.2 Dissipation of the kinetic energy scale for 2D flow

Farge et al. [1], one of the first authors who investigated the dissipations of the kinetic energy and its relationship with the growth of the enstrophy . They applied that the dissipation of the energy persists in the vanishing viscosity limit. From the evaluation of the dipole wall collision, one can see two regimes. The first one appears before the first wall collision, from $t = 0$ until a boundary layer at the wall appears where the dipole is close to the wall around $t = 0.3$. Here, the effects of the boundary layer are neglected. So according to equation (38), the energy dissipation scales fulfill the following

$$E(t_2) - E(t_1) \propto \frac{1}{Re}. \tag{40}$$

The second regime is placed when the two cores of vortices are close to the boundary where the secondary vortices start to induce by the effect of the first wall collision around $t = 0.3$. In this regime, the Prandtl's theory is satisfied [10]. From this theory, we can see the boundary layer of thickness scales of order $Re^{-0.5}$. Thus in the second regime, the dissipation of the energy scale is

$$E(t_2) - E(t_1) \propto Re^{-\frac{1}{2}}. \tag{41}$$

The growth of the enstrophy scale will depend on the relationship of equations (38) and (39) thus

$$\Psi(t_2) - \Psi(t_1) \propto Re \tag{42}$$

In this section, we present two cases of incidents, the normal wall collision and an oblique wall collision at an angle of $30°$.

7.2.1 Dissipation of the kinetic energy for normal wall incident

In this section, we study the energy dissipation rate of the dipole that collides with the wall normally. For the two regimes, as a function of Reynolds number in a range of $Re = 250$ to $Re = 10000$, the dissipation of the kinetic energy will be investigated. When the dipole is at a long distance from the wall, the first regime is identified in the time interval $t \in [0: 0.2]$. The study of average dissipation is carried out for no slip and slip boundaries for various values of slip length. As can be seen in Figure 4, For different values of slip length the dissipation of the energy collapses in one line on a scale of Re^{-1}. Noting, that the energy dissipation and the growth of the enstrophy will be divided by $\Delta(t) = (t_2 - t_1)$.

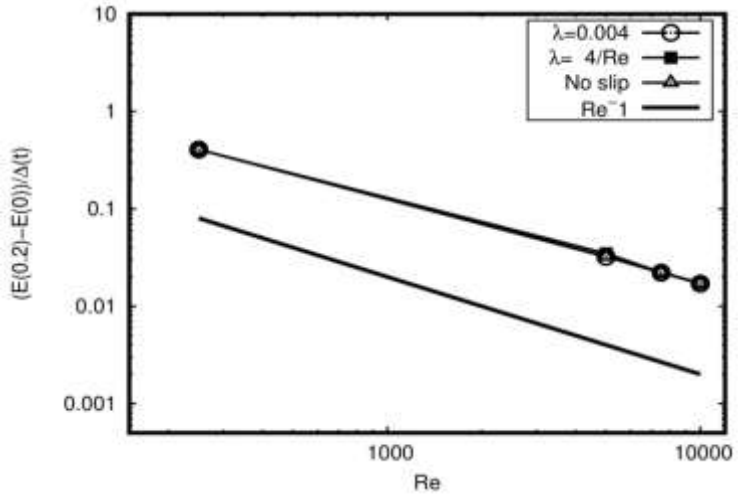

Figure 4: Energy dissipation for normal collision in the first regime, $\mathbf{0} < \boldsymbol{t} < \mathbf{0.2}$. The dissipation for slip length: λ=0.004, λ =4/Re and no slip cases are shown.

When the dipole reaches the wall, the second regime will be chosen. In this area, the boundary layer will be induced as a result of the interaction between the two monopoles and the boundary. Therefore Prandtl's theory will be satisfied. Following [9][15], we choose the time interval that satisfies Prandtl's theory when the dipole starts to collide with the wall. Once we identify the time period, we start to investigate the dissipation of the energy and the growth of the enstrophy. The investigation shows that the dissipation of the energy fulfills Prandtl's theory. First, we considered $\lambda = 0.004$. The best choice of time interval is when the boundary layer appears near the wall at $t = 0.23$ and it ends when the dipole separates from the wall at $t = 0.47$. After we choose the correct time interval, we test the validation of the theory. As a results, we found that the decay of the energy rate is $\frac{\Delta E}{\Delta t} \propto Re^{-0.5}$. Thus Prandtl's theory is achieved. For the corresponding enstrophy growth for $\lambda = 0.004$ we show it satisfies $\frac{\Delta \Psi}{\Delta t} \propto Re$ for Reynolds numbers higher than 2500. The results are shown in Figure 5.

(a) Energy dissipation (b) Enstrophy growth

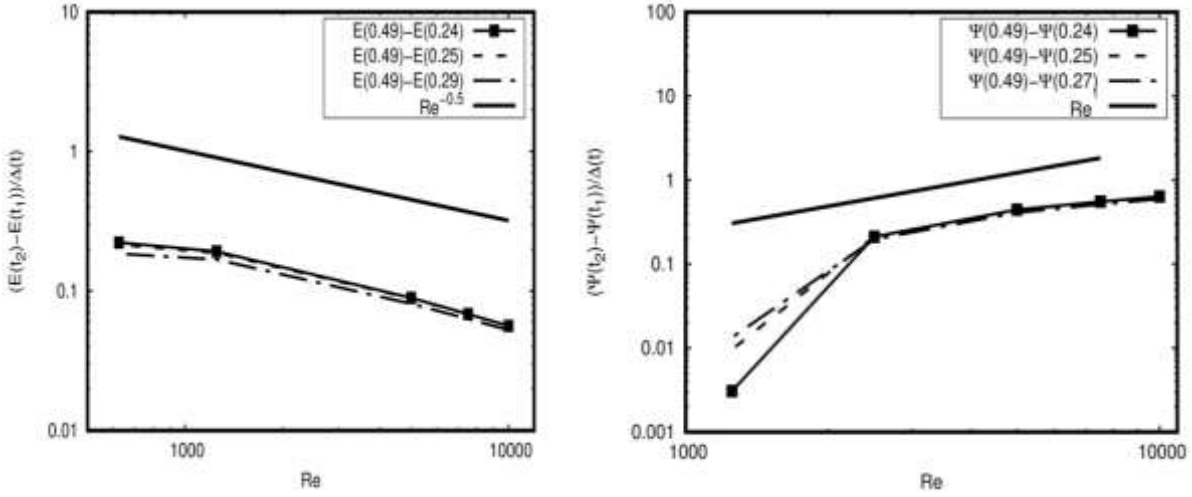

Figure 5: $\frac{\Delta E}{\Delta t}$ and $\frac{\Delta \Psi}{\Delta t}$ at $\boldsymbol{\lambda = 0.004}$ for normal wall collision

Second, we test the theory for no slip wall and a boundary with slip length that depends on the Reynolds number such that $\lambda = 4/Re$. The last value of slip length is chosen for sake of comparison with Sutherland [9], Mohammed [15] and Frag et al. [1] . We found an excellent agreement between our results and the findings in these papers. For both cases, the time interval will be between $t = 0.2$ and $t = 0.49$. Noting, that the same technique is used for all slip lengths to find the best time interval for the second regime. Figures 6 and 7 show the kinetic energy dissipation and growth of enstrophy scales for these two cases. These figures illustrate that the dissipation of the energy scale is proportional to $Re^{-\kappa}$ where $\kappa \propto 0.5$ for $Re \geq 1252$ and 0.43 for $Re < 1252$. These results synchronize with the difference of enstrophy growth such that $\Delta\Psi \propto Re$ for higher Reynolds numbers.

(a)) Energy dissipation (b) Enstrophy growth

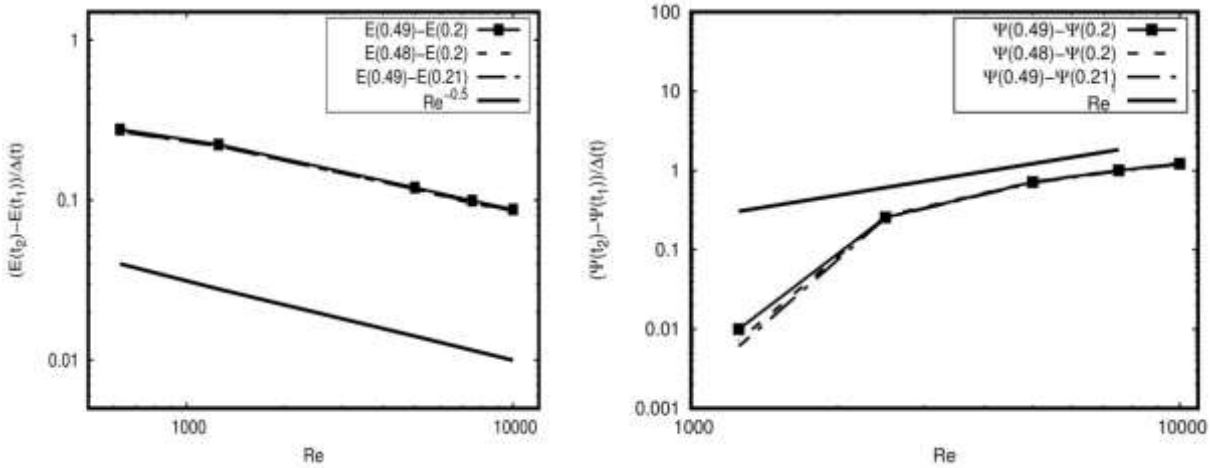

Figure 6: $\frac{\Delta E}{\Delta t}$ and $\frac{\Delta \Psi}{\Delta t}$ for no-slip for normal dipole wall collision.

(a)) Energy dissipation (b) Enstrophy growth

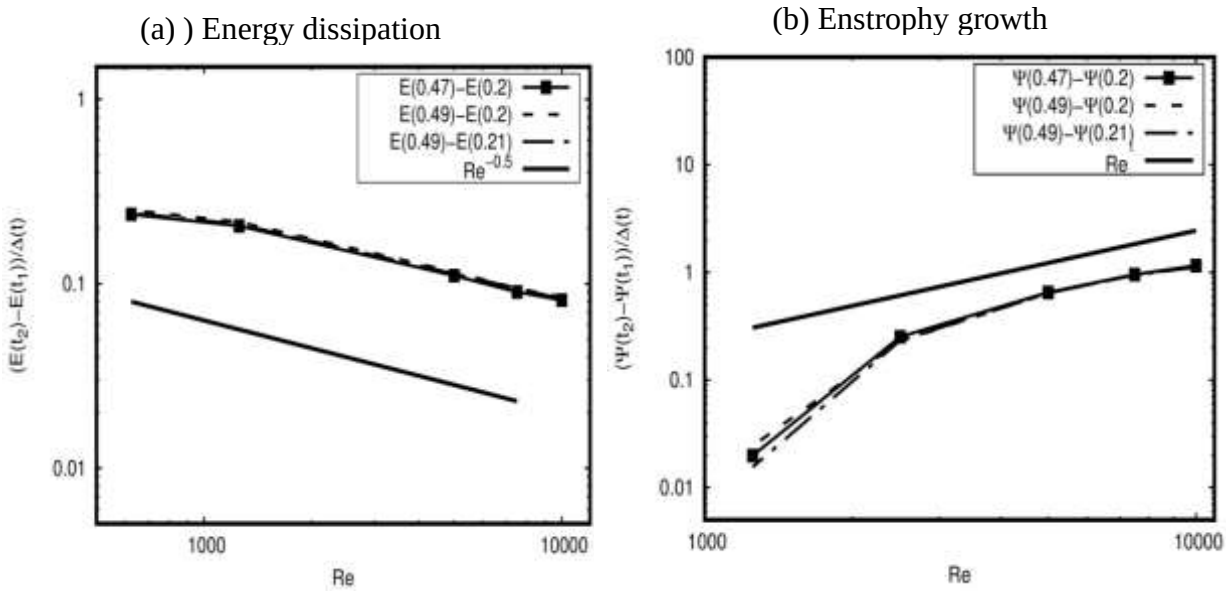

Figure 7: $\frac{\Delta E}{\Delta t}$ and $\frac{\Delta \Psi}{\Delta t}$ at $\lambda = \frac{4}{Re}$ for normal dipole wall collision**.**

7.2.2 Dissipation of the kinetic energy for oblique -30° wall collision case

In this subsection, the dissipation of the kinetic energy with the growth of the enstrophy rates will be performed for dipole wall collision at an angle of 30^{o} with an initial location (0.0839,0.0866);(0.1839, -0.086). In this case, as at normal wall collision, the rate will be

discussed for no slip and slip walls with slip length $\lambda = 0.004$ and $\lambda = \frac{4}{Re}$. For an oblique collision, The first regime is located from $t = 0$ until $t = 0.2$ which is before the boundary layer appears near the east wall. Similar to the normal collision, three lines for various slip lengths collapse in one slop where $\Delta E(t) \propto Re^{-1}$, see Figure 8

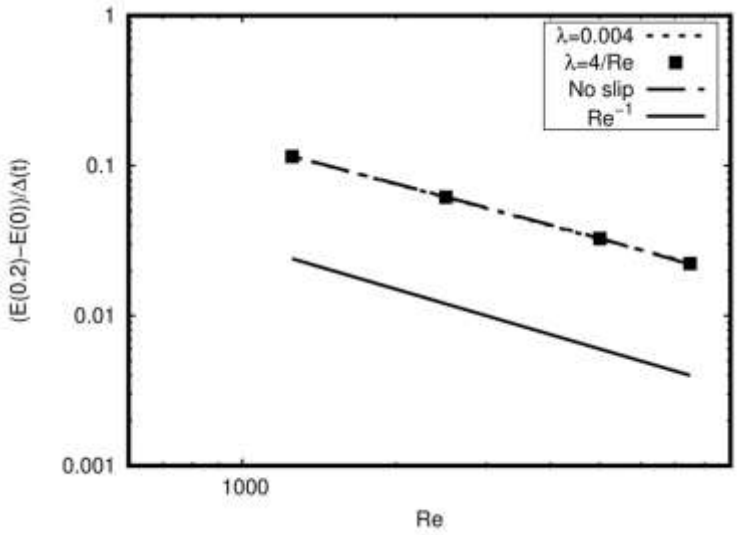

Figure 8: Energy dissipation for oblique-$\mathbf{30}^{\circ}$ collision in the first regime, 0<t<0.2. The dissipa tion for slip length: λ=0.004, λ =4/Re and no slip cases are shown.

At the second regime, the two monopoles reach the wall approximately around $t = 0.3$. We use the same time intervals that we applied for normal wall collision since the bottom core of the vortices hit the wall at this time step. Figure 9 shows the dissipation of the kinetic energy and the growth of enstrophy rates for an oblique case close to the wall for $\lambda = 0.004, 4/Re$ and no slip cases for $t \in [0.21,0.48]$. As a result, the dissipation of the kinetic energy is consistent with Prandtl's theory and the growth of enstrophy increases linearly with Re at higher Reynolds numbers.

(a) Energy dissipation (b) Enstrophy growth

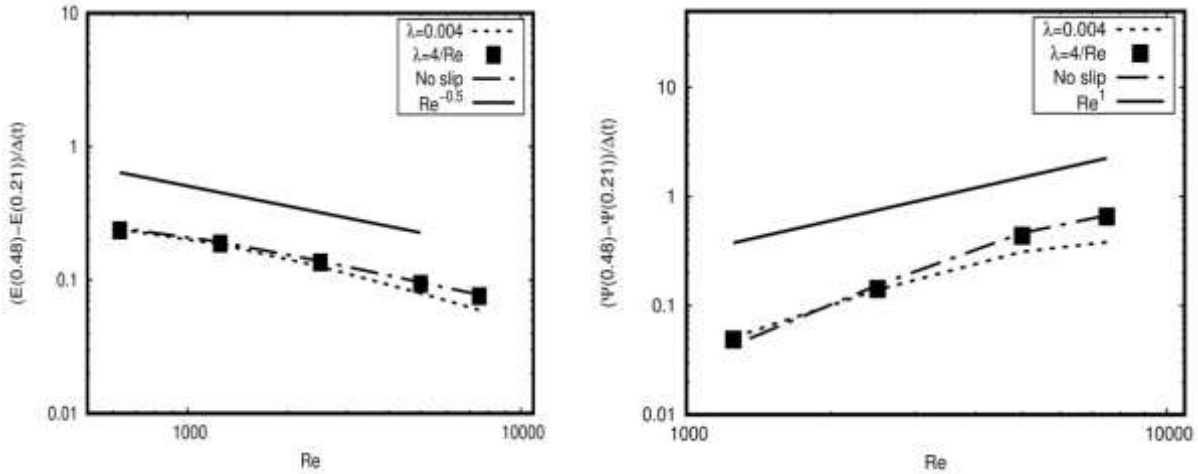

Figure 9: Energy dissipation and enstrophy growth for for oblique-30◦ dipole wall collision for the second stage of collision.

Conclusions

The lattice Boltzmann method with two relaxation time model has been used to examine the dissipation of the kinetic energy and the growth of enstrophy for 2D fluid flow. For precision reasons, we set the "magic parameter $\Lambda = \frac{1}{4}$ in the TRT-LBE model. No slip and Maxwell slip velocity conditions under the effect of Burnett- order deviatoric stress conditions were imposed on stationary walls using the Moment-based method. The numerical study was implemented for median and higher Reynolds numbers. Also, it was performed for fixed slip length and $\lambda = 4/Re$ for the sake of comparison. The given approach captured the dissipation rate accurately for two angles of collisions and proved that the dissipation of the energy is proportional to enstrophy. The examination includes two regimes. The first one showed that the dissipation rate is proportional to Re^{-1} while $\frac{dE}{dt} \propto Re^{-0.5}$ when the boundary layer appearance is dominant. In this stage and according to the relationship in equation (38) we found $\Delta\Psi \propto Re$. This method showed an excellent agreement with other benchmark methods.

References

[1] M. Farge, K. Schneider and K. Schneider, "Energy dissipating structures produced by walls in two-dimensional flows at vanishing viscosity," *Physical Review Letters*, vol. 106, no. 18, p. 184502, 2011.

[2] H.J.H. Clercx and C.-H. Bruneau, "The normal and oblique collision of a dipole with a no-slip boundary,"*Computers & fluids*, vol.35, no. 3, pp. 245-279, 2006.

[3] S. Mohammed, D. Graham and T. Reis," Assessing moment-based boundary conditions for the lattice Boltzmann equation: A study of dipole-wall collisions," *Computers & Fluids*, vol. 176, pp. 79–96, 2018.

[4] S. Mohammed and T. Reis, "Modeling the effects of slip on dipole–wall collision problems using a lattice Boltzmann equation method," *Physics of Fluids***,** vol. 32, no. 2, p. 025104, 2020.

[5] P. Orlandi,"Vortex dipole rebound from a wall," *Physics of Fluids A*: *Fluid Dynamics*, vol 2, no. 8, pp. 1429-1436, 1990.

[6] J. Latt and B. Chopard," A benchmark case for lattice Boltzmann: turbulent dipole-wall collision," *International Journal of Modern Physics C*, vol 18, no. 04, pp. 619-626, 2007.

[7] H.J.H. Clercx and G.J.F. van Heijst," Dissipation of kinetic energy in two-dimensional bounded flows," *Physical Review E*, vol. 65, no. 6, p. 066305, 2002.

[8] G.H. Keetels, W. Kramer, H.J.H Clercx and G.J.F. van Heijst, "On the Reynolds number scaling of vorticity production at no-slip walls during vortex-wall collisions," *Theoretical and computational fluid dynamics*, vol. 25, no. 5, pp. 293-300, 2011.

[9] D. Sutherland, C. Macaskill and D.G. Dritschel," The effect of slip length on vortex rebound from a rigid boundary," *Physics of Fluids (1994-present)*, vol. 25, no. 9, p. 093104, 2013.

[10] L. Prandtl," Uber ussigkeitsbewegung bei sehr kleiner reibung," *Verhandl. III, International Math-Kong, Heidelberg, Teubner, Leipzig*, pp. 484-491, 1904.

[11] H.J.H Clercx and G.J.F. van Heijst," Dissipation of coherent structures in confined two-dimensional turbulence," *Physics of Fluids*, vol. 29, no. 11, p. 111103, 2017.

[12] J. A. Al-Hawasy and M.A Jawad," Approximation Solution of Nonlinear Parabolic Partial Differential Equation via Mixed Galerkin Finite Elements Method with the Crank-Nicolson Scheme," *Iraqi Journal of Science*, vol. 60, no. 2, pp. 353-361,2019.

[13] A. Hammodat, G. Algwauish and I. Al-Obaidi," The Effects of Electrical Conductivity on Fluid Flow between Two Parallel Plates in a Porous Medioum," *Iraqi Journal of Science*, vol. 62, no. 12, pp. 4953-4963,2021.

[14] A.M. Abdulhadi and A.H. Al-hadad," Slip Effect on the Peristaltic Transport of MHD Fluid through a Porous Medium with Variable Viscosity," *Iraqi Journal of Science*, vol. 56, no. 3B, pp. 2346-2363,2015.

[15] S. Mohammed," The lattice Boltzmann method for slip and no-slip boundaries." PhD dissertation, Dept of Math. Sci. Univ. Of Plymouth, UK, 2019.

[16] X. He and L. Luo, "A priori derivation of the lattice Boltzmann equation," *Physical Review E*, vol. 55, no. 6, p. R6333 ,1997.

[17] X. Shan, X. Yuan and H. Chen,"Kinetic theory representation of hydrodynamics: A way beyond the Navier–Stokes equation," *Journal of Fluid Mechanics*, vol. 550, pp. 413–441 ,2006.

[18] S. Succi, *The lattice Boltzmann equation: for fluid dynamic and beyond*, Oxford university press.,2011

[19] D. d'Humieres," Generalized lattice-Boltzmann equations," *Rarefied gas dynamics*, pp. 450–458, 1992.

[20] I. Ginzburg ,"Lattice Boltzmann modeling with discontinuous collision com- ponents: Hydrodynamic and advection-diffusion equations," *Journal of Statistical Physics*, vol. 126, no. 1, pp. 157–206, 2007 .

[21] I. Ginzburg." Equilibrium-type and link-type lattice Boltzmann models for generic advection and anisotropic-dispersion equation," *Advances in water resources*, vol. 28, no. 11, pp. 1171–1195, 2005 .

[22] I. Ginzburg , D. d'Humières and A Kuzmin,"Optimal stability of advection-diffusion lattice Boltzmann models with two relaxation times for positive/negative equi- librium" *Journal of Statistical Physics*, vol. 139, no. 6, pp. 1090–1143, 2010 .

[23] YH. Qian, D. d'Humières and P. Lallemand, "Lattice BGK models for Navier-Stokes equation," *Europhysics letters*, vol. 17, no. 6, p. 479, 1992.

[24] Z. Guo and C. Shu, *Lattice Boltzmann method and its applications in engineering*, World Scientific, 2013.

[25] J.E. Broadwell, " Study of rarefied shear flow by the discrete velocity method," *Journal of Fluid Mechanics*, vol. 19, no. 3, pp. 401–414, 1964.

[26] R. Gatignol, "Kinetic theory boundary conditions for discrete velocity gases." *Phys. Fluids (1958-1988)*, vol. 20, no. 12, pp. 2022–2030, 1977.

[27] S. Ansumali and I. V Karlin. "Kinetic boundary conditions in the lattice Boltzmann method." *Physical Review E*, vol. 66, no. 2, p. 026311, 2002.

[28] Q. Zou and X. He, "On pressure and velocity boundary conditions for the lattice Boltzmann BGK model." *The Physics of Fluids*, vol. 9, no. 6, pp. 1591–1598, 1997.

[29] D.R. Noble, S. Chen, G. Georgiadis and R. O. Buckius, "A consistent hydrodynamic boundary condition for the lattice Boltzmann method," *The Physics of Fluids*, vol. 7, no. 1, pp. 203–209, 1995.

[30] S. Bennett. A lattice Boltzmann model for diffusion of binary gas mixtures. PhD dissertation, University of Cambridge, UK, 2010.

[31] R. Allen and T. Reis, "Moment-based boundary conditions for lattice Boltzmann simulations of natural convection in cavities Progress in Computational Fluid Dynamics, an International Journal, vol. 16, no. 4, pp. 216–231, 2016.

[32] A. Hantsch, T. Reis and U. Gross," Moment method boundary conditions for multiphase lattice Boltzmann simulations with partially-wetted walls," *The Journal of Computational Multiphase Flows*, vol. **7**, no. 1, pp. 1–14 ,2015.

[33] S. Mohammed and T. Reis,"Using the lid-driven cavity flow to validate moment-based boundary conditions for the lattice Boltzmann equation," *Archive of Mechanical Engineering*, vol. 64, no. 1, pp. 57–74 ,2017.

[34] T. Reis, " Burnett order stress and spatially-dependent boundary conditions for the lattice Boltzmann method," *Progress in Computational Fluid Dynamics, an International Journal Commun. Comput. Phys,* vol. 27, pp. 167–197 ,2020.

[35] T. Reis, "On the Lattice Boltzmann Deviatoric Stress: Analysis, Boundary Conditions, and Optimal Relaxation Times," *SIAM Journal on Scientific Computing,* vol. 42, no. 2, pp. 397-424, 2020.

[36] S. Mohammed and T. Reis," A Lattice Boltzmann method with moment-based boundary conditions for rarefied flow in the slip regime," *Physical Review E,* vol. 1.4, no. 4, p. 045309,2021.

[37] X. He and L-S Luo, "Theory of the lattice Boltzmann method: from the Boltzmann equation to the lattice Boltzmann equation," *Physical Review E,* vol. 56, no. 6, p. 6811, 1997.

[38] S. Chapman and Th. G. Cowling, *The mathematical theory of non-uniform gases: an account of the kinetic theory of viscosity, thermal conduction and diffusion in gases*, (Cambridge University Press, Cambridge, England, 1970.

[39] E. Ikenberry and C. Truesdell, "On the pressures and the flux of energy in a gas according to maxwell's kinetic theory, I," *Journal of Rational Mechanics and Analysis*, vol. 5, no. 1, pp. 1-54, 1956.

[40] X. He, X. Shan and G.D. Doolen," Discrete Boltzmann equation model for nonideal gases," *Physical Review E*, vol. 57:R13, no. 1, 1998.

[41] P.J. Dellar, "Incompressible limits of lattice Boltzmann equations using multiple relaxation times," *Journal of Computational Physics*, vol. 190, no. 2, pp. 351–370, 2003.

[42] P. Lallemand and L.S. Luo, "Theory of the lattice Boltzmann method: Dispersion, dissipation, isotropy, Galilean invariance, and stability," *Physical Review E.*, vol. no. 61, pp. 6546, 2000.

[43] J. Latt and B. Chopard, " Lattice Boltzmann method with regularized non- equilibrium distribution functions,"*arXiv preprint physics,* p. 0506157, 2005.

[44] D. D'Humieres and I. Ginzburg,"Viscosity independent numerical errors for lattice Boltzmann models: from recurrence equations to magic collision numbers," *Computers & Mathematics with Applications*, vol. 58, no. 5, pp. 823-840, 2009.

[45] C. Navier, *Memoire sur les lois du mouvement des fluids*," *Memoires de l'Academie Royale des Sciences*, vol. 6 , pp. 389–440, 1823.